

Structural, optical and magnetic properties of $\text{Bi}_{0.9-y}\text{Sm}_y\text{La}_{0.1}\text{FeO}_3$ thin films deposited by pulsed laser deposition technique

A. KAUSHAL^a, D. KAUR^b, N. KUMAR^{c,*}

^aDepartment of Ceramic and Glass Engineering, University of Aveiro, Aveiro, Aveiro-3810-193, Portugal

^bDepartment of Physics and Centre of Nanotechnology, Indian Institute of Technology Roorkee, Roorkee-247667, India

^cDepartment of Physics, LIT-Engineering, Lovely Professional University Phagwara, Punjab-144402, India

We report on the synthesis of BiFeO_3 (BFO) and $\text{Bi}_{0.9-y}\text{Sm}_y\text{La}_{0.1}\text{FeO}_3$ (BSLFO) ($y = 0, 0.02$ and 0.1) thin films on quartz substrate using pulsed laser deposition (PLD) technique. The effect of doping Sm in $\text{Bi}_{0.9}\text{La}_{0.1}\text{FeO}_3$ (BLFO) on structural, optical and magnetic properties has been systematically investigated. X-ray diffraction (XRD) measurement shows the rhombohedral structure for the deposited films with highly oriented (110) diffraction peak. Atomic force microscopy (AFM) of the films reveals the decrease in grain size with corresponding increase in Sm composition. Magnetic studies shows the ferromagnetism with Sm doping in BLFO with saturation magnetization 17.5 emu/cm^3 and coercivity 121 Oe in case of $\text{Bi}_{0.9-y}\text{Sm}_y\text{La}_{0.1}\text{FeO}_3$ ($y = 0.1$) thin film at room temperature. However, antiferromagnetic behavior has been found in case of BFO. The M-T curve shows a large enhancement in magnetism of BLFO thin films by the addition of Sm. Optical measurement reveals the decrease in refractive index with Sm doping. Moreover, a red shift in band gap calculation has been found with increase in Sm doping in BLFO which provide a reference for preliminary research to infrared detectors and optoelectronic devices.

(Received March 29, 2011; accepted May 31, 2011)

Keywords: $\text{Bi}_{0.9-y}\text{Sm}_y\text{La}_{0.1}\text{FeO}_3$, Thin films, Optical band gap, AFM, PLD technique

1. Introduction

Multiferroic materials, in which ferroelectricity and magnetism coexist are currently gaining much attention due to their potential application in devices taking advantage of two coupled degrees of freedom based on local lattice distortion and electron spin and allow a direct integration of the material into the up-to-date semiconductor technology. Multiferroic oxide thin films are intensively investigated because of their scientific importance and technological promise for applications as non-volatile memories, such as ferroelectric random-access memories (FeRAM) and magnetoresistive random-access memories (MRAM) etc. [1, 2]. Among various multiferroic oxide materials, BiFeO_3 (BFO) has attracted much attention because of its high Curie temperature, $T_C = 830 \text{ }^\circ\text{C}$, and its high Néel temperature, $T_N = 370 \text{ }^\circ\text{C}$ [3]. Powder X-ray diffraction (XRD) and neutron diffraction studies revealed that BiFeO_3 has a rhombohedrally distorted perovskite structure [4, 5]. The inhomogeneous magnetic spin structure of BiFeO_3 leads to the cancellation of macroscopic magnetization and inhibits the observation of the linear magnetoelectric effect. Enhancement of magnetization has been observed in $\text{Bi}_{1-x}\text{R}_x\text{FeO}_3$ ($\text{R} = \text{Nd}^{3+}$, Tb^{3+} etc) [6, 7]. Similarly the multiferroic properties have been enhanced for La doping in BiFeO_3 [8, 9]. V.R. Palkar et al [10] has reported the doping of Tb and La and discovered the coexistence of ferroelectricity and

ferromagnetism along with high dielectric constant and magnetoelectric coupling at room temperature.

Although there are reports on BFO thin films using wet chemical method [11, 12], we prefer to deposit films by PLD due to its added advantage of being a non-equilibrium process. Moreover, PLD has been recognized as a promising versatile technique for the deposition of stoichiometric films of metal oxides at high deposition rate [13]. Earlier we have reported the effect of La doping on various properties of BiFeO_3 thin films deposited by PLD technique [14]. In the present study, we have investigated the effect of Sm doping on structural, optical and magnetic properties of BiLaFeO_3 (BLFO) thin films deposited on quartz substrate using PLD technique. A red shift in band gap calculation has been found with increase in Sm doping in BLFO. Magnetic behavior has been found to be improved with Sm doping in BLFO with enhancement in saturation magnetization and remanent magnetization. Also, the optical properties of the deposited films are investigated which provide a reference for preliminary research into infrared detectors and optoelectronic devices. The optical band gap was found to decrease from 2.66 eV to 2.54 eV with corresponding increase in Sm composition from $y = 0$ to $y = 0.1$ in $\text{Bi}_{0.9-y}\text{Sm}_y\text{La}_{0.1}\text{FeO}_3$ films.

2. Experimental details

Thin films of BiFeO_3 and $\text{Bi}_{0.9-y}\text{Sm}_y\text{La}_{0.1}\text{FeO}_3$ with $y = 0, 0.02$ and 0.1 were grown on quartz substrates by

pulsed laser deposition technique using 15 mm diameter targets. The details of process setup are given elsewhere [13]. The targets were prepared by mixing appropriate molar ratios of Bi_2O_3 , Fe_2O_3 , La_2O_3 and Sm_2O_3 powders. After 8 hours of grinding, the mixed powder was calcined in air at 600 °C for 2 hours. The powder was further reground and pressed into pellets by applying pressure of 80 MPa. Finally, it was sintered at 870 °C for 5 minutes by rapid thermal process. The KrF excimer laser (248 nm, 10 Hz) with energy of 300 mJ was used for the deposition of films. The substrate temperature was maintained at 600 °C with oxygen pressure of 50 mTorr and deposition time of 35 minutes. Before ablation, the chamber was evacuated to a base pressure of 10^{-6} Torr, and then the pure oxygen was introduced through a mass flow controller. The chamber pressure was measured using a combination vacuum gauge (Pfeiffer Vacuum) and maintained at a pressure of 50 mTorr. Before every deposition, the target was pre-ablated for 1 minute in order to ascertain the same state of the target in every deposition. After the deposition, the films were annealed at 700 °C for 30 minutes for crystallization. The films were allowed to cool in the chamber naturally and then characterized for its properties using various techniques.

3. Results and discussion

3.1 Structural properties

Fig. 1 shows the XRD pattern for undoped BiFeO_3 and $\text{Bi}_{0.9-y}\text{Sm}_y\text{La}_{0.1}\text{FeO}_3$ ($y = 0, 0.02, 0.1$) thin films deposited at quartz substrates. XRD measurements shows the rhombohedral structure for the deposited films with highly oriented (110) diffraction peak which are in confirmation of earlier reports [15, 16]. A few low intensity additional peaks at $2\theta = 28.32$ and 29.12 has also been observed in the XRD pattern for undoped BiFeO_3 films. The presence of these low intensity peaks could be attributed to impurity peaks due to the formation of $\text{Bi}_2\text{Fe}_4\text{O}_9$, which eliminates on doping with La and Sm. Moreover, the Sm doping in BLFO leads to growth of low intensity (-220) and (010) diffraction peaks. The crystallite size calculated from XRD patterns using well known Scherer's formula [17] have been found to increase from 24.62 nm to 31.76 nm with corresponding doping in undoped BFO with La. However, Sm doping in La doped BFO films shows a decrease in crystallite size from 31.76 nm to 29.62 nm with corresponding increase in Sm content from $y=0$ to $y=0.1$ as shown in Table 2. This type of variations in crystallite size could be attributed to the difference in ionic radii of Bi^{3+} (103 pm), La^{3+} (103.2 pm) and Sm^{3+} (95.8 pm).

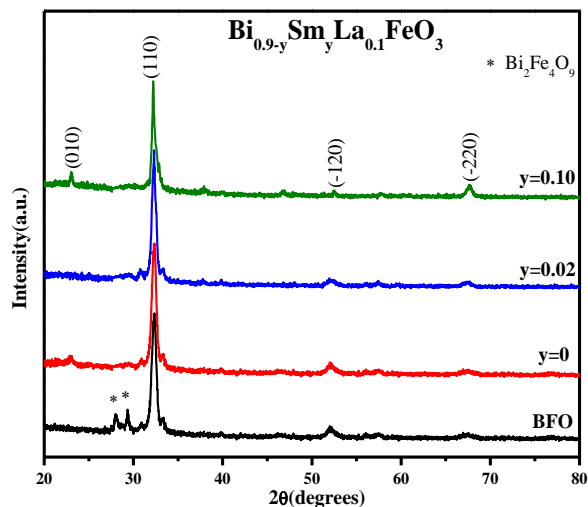


Fig. 1. XRD pattern of BiFeO_3 and $\text{Bi}_{0.9-y}\text{Sm}_y\text{La}_{0.1}\text{FeO}_3$ thin films of different Sm contents (y).

From XRD patterns, it is clear that La and Sm addition provides phase purity and stabilizes the perovskite structure. Our measurements suggests the elimination of secondary phases is due to the effect of doping which can be qualitatively substantiated with the thermodynamics along with Pauling's equation [18] that relates ionic bond strength (I_{AB}) with the average electronegativity of cation (χ_A) and anion (χ_B) as given in following equation:

$$I_{AB} = 1 - \exp[-(\chi_A - \chi_B)/4] \quad (1)$$

Table 1 shows the electronegativity values of various A-site cations (Bi^{3+} , La^{3+} , Sm^{3+}) and anion (O^{2-}) and the values of ionic bond strength calculated using above equation. The calculated values suggest that the ionic bond strength of La-O and Sm-O bond is higher than that of Bi-O bond. This may lead to reduced enthalpy of formation (ΔH_f) of La and Sm doped BiFeO_3 as compared to undoped BiFeO_3 as ΔH_f is a function of bond strength ($\Delta H_f = \text{PAB} (\epsilon_{AB} - (\epsilon_{AA} + \epsilon_{BB})/2)$ where PAB is the number of A-B bonds and ϵ represents that bond energy which becomes increasingly more negative as the bond strength increases). This can reduce the free energy of formation (ΔG_f) of La and Sm doped BiFeO_3 phase as compared to undoped BiFeO_3 phase. ΔG_f may become more negative if entropy change is positive considering La-O and Sm-O bond replaces Bi-O bond in the lattice randomly. This will make La and Sm doped BiFeO_3 phase more stable than undoped BiFeO_3 .

Table 1. Calculated ionic bond strength of Bi-O, La-O and Sm-O bond.

Species	Electronegativity	Ionic bond Strength with O^{2-} (electronegativity = 3.44)
Bi^{3+}	2.02	0.30
La^{3+}	1.1	0.44
Sm^{3+}	1.17	0.43

Fig. 2 shows the AFM images of BFO and BSLFO thin films with scan area of $1 \mu\text{m} \times 1 \mu\text{m}$. The images shows an increase in grain size with La doping in BFO thin films and decrease in grain size with corresponding Sm doping in BLFO thin films. The AFM results are in agreement with the XRD results.

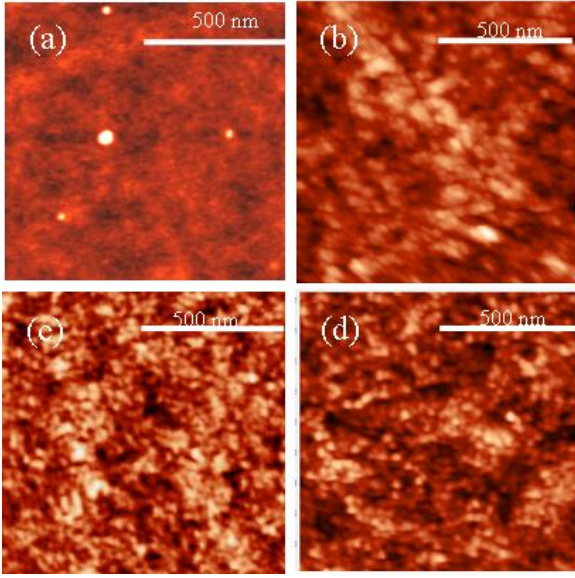


Fig. 2. AFM micrographs of (a) undoped BiFeO_3 and $\text{Bi}_{0.9-y}\text{Sm}_y\text{La}_{0.1}\text{FeO}_3$ thin films with (b) $y = 0$, (c) $y = 0.02$ and (d) $y = 0.1$.

3.2 Optical properties

Fig. 3 shows the optical transmission spectra of undoped BFO and BSLFO thin films with Sm content $y = 0$, $y = 0.02$ and $y = 0.1$ in the wavelength range from 200 nm to 2000 nm. All the films are highly transparent with an average transmittance of about 75 %. A gradual shift of transmission edge towards a longer wavelength with increase in Sm content was observed. The refractive index (n) was calculated from the transmission spectrum by using the following expression [19]:

$$n = \left[N + \left(N^2 - n_0^2 n_1^2 \right)^{1/2} \right]^{1/2}, \quad (2)$$

Where

$$N = \frac{n_0^2 + n_1^2}{2} + 2n_0 n_1 \frac{T_{\max} - T_{\min}}{T_{\max} T_{\min}} \quad (3)$$

and n_0 and n_1 (1.46 in our case) are the refractive index of air and substrate, respectively. T_{\max} and T_{\min} are maximum and minimum transmittance values at the same wavelength. Fig. 4 represents the refractive indices (n) variation with wavelength (λ) for the undoped BFO and BSLFO films of different Sm composition. Refractive indices of all the films decreases with increase in wavelength, thus give the normal dispersion behavior. The refractive index for undoped BiFeO_3 and $\text{Bi}_{0.9}\text{La}_{0.1}\text{FeO}_3$ at wavelength of 700 nm was found to be 2.10 and 2.30 respectively. However, it has been found that the refractive index decreases from 2.30 to 1.97 with corresponding increase in Sm content from $y = 0$ to $y = 0.1$. The calculated results are shown in Table 2. The decrease in refractive index is accompanied by a decrease in density of the material by addition of Sm [20].

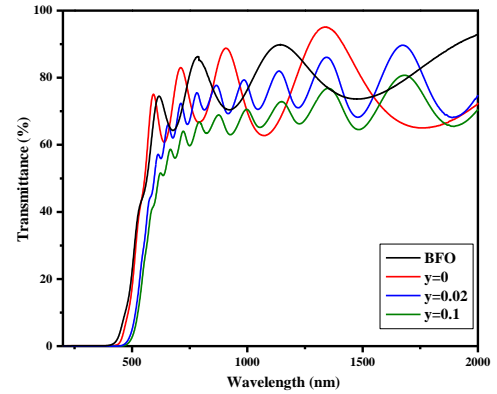


Fig. 3. Transmittance of BiFeO_3 and $\text{Bi}_{0.9-y}\text{Sm}_y\text{La}_{0.1}\text{FeO}_3$ thin films of different Sm contents (y).

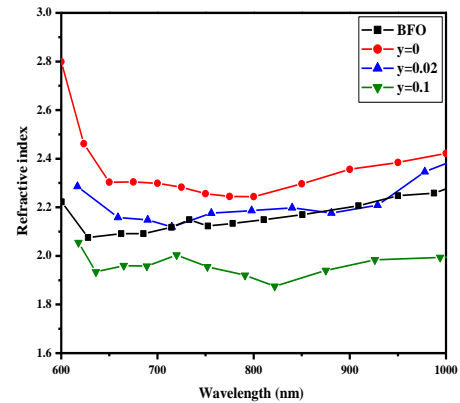


Fig. 4. Refractive index variations with wavelength of BiFeO_3 and $\text{Bi}_{0.9-y}\text{Sm}_y\text{La}_{0.1}\text{FeO}_3$ thin films of different Sm contents (y).

Table 2. Calculated crystallite size, refractive index and band gap of BiFeO₃ and Bi_{0.9-y}Sm_yLa_{0.1}FeO₃ thin films with different Sm content (y).

Sample	Sm Contents (y)	Crystallite Size (nm)	Refractive Index at 700 nm	Optical Band Gap (eV)
BiFeO ₃	0	24.62	2.10	2.68
Bi _{0.9-y} Sm _y La _{0.1} FeO ₃	0	31.76	2.30	2.66
	0.02	31.58	2.16	2.57
	0.1	29.62	1.97	2.54

The optical absorption coefficient α is calculated from the following relation [21]:

$$T = \frac{(1-R)^2 \exp(-\alpha t)}{1-R^2 \exp(-2\alpha t)} \quad (4)$$

where R and T are the spectral reflectance and transmittance and t is the film thickness. For greater optical density ($\alpha t > 1$), the interference effects due to internal reflections as well as reflectance at normal incidence are negligible, and the previous equation can be approximated as

$$T \approx \exp(-\alpha t) \quad (5)$$

The optical absorption coefficient α is given by the approximate formula,

$$\alpha = -\frac{1}{t} \ln T \quad (6)$$

where t is the film thickness and T the transmittance measured. The direct and indirect band gap of the films was calculated using the Tauc relationship as follows [22]:

$$\alpha h\nu = A(h\nu - E_g)^n \quad (7)$$

where α is the absorption coefficient, A is a constant, h is the Planck's constant, ν is the photon frequency, E_g is the energy band gap and n is $\frac{1}{2}$ for direct band gap semiconductor. An extrapolation of the linear region of a plot of $(\alpha h\nu)^{\frac{1}{n}}$ on the y-axis versus photon energy ($h\nu$) on the x-axis gave the value of the energy band gap E_g .

Since $E_g = h\nu$ when $(\alpha h\nu)^{\frac{1}{n}} = 0$, here the direct band gaps for the BFO and BSLFO thin films were evaluated by extrapolating the straight line part of the curves $(\alpha h\nu)^2 = 0$ as shown in Fig. 5. The La addition in BiFeO₃ causes the band gap to decrease from 2.68 eV to

2.66 eV. The value of direct band gap further decreases from 2.66 eV to 2.54 eV with corresponding increase in Sm content from $y = 0$ to $y = 0.1$ as shown in Table 2. The observed red shift in band gap could be attributed to the compositional change on addition of Sm in Bi_{0.9}La_{0.1}FeO₃. In the fundamental absorption region, the absorption is due to the transition from the top of valence band to the bottom of the conduction band. Sm doping in Bi_{0.9}La_{0.1}FeO₃ thin film may cause an increase in the density of state in the valence band. The addition of Sm may also create localized states in the band gap which lead to a shift in the absorption edge towards lower photon energy, and, thus a decrease in the optical energy gap.

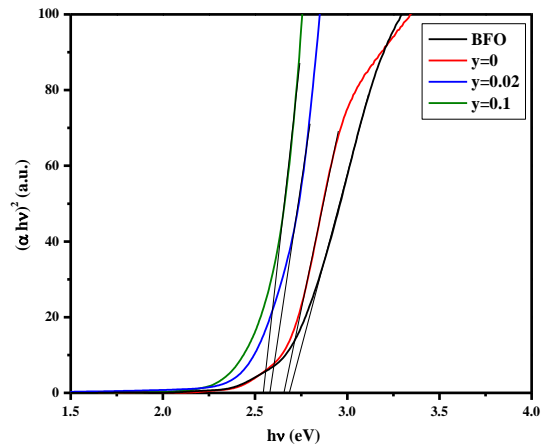


Fig. 5. $(\alpha h\nu)^2$ vs. $h\nu$ plot of BiFeO₃ and Bi_{0.9-y}Sm_yLa_{0.1}FeO₃ thin films of various Sm contents.

3.3 Magnetic properties

Fig. 6 shows the magnetization (M) versus applied field (H) of BFO and BSLFO thin films with Sm composition $y = 0$ and $y = 0.1$ at temperatures 5 K and 300 K respectively. At 300 K, the magnetization for undoped BiFeO₃ is very small and varies almost linearly with the field as expected for an antiferromagnetic material. There is no sign of saturation found in it. The small

magnetization is due to spin canting in the antiferromagnetic BiFeO_3 . With the addition of La into BiFeO_3 , the magnetization curve saturates at a value 6.8 emu/cm^3 , and there is an increase in coercivity from 94 Oe to 202 Oe. There is an enhancement in remanent magnetization from 0.26 emu/cm^3 to 1.86 emu/cm^3 as shown in Table 3. With the addition of Sm into BLFO, the saturation magnetization increases from 6.8 emu/cm^3 to 17.5 emu/cm^3 and remanent magnetization increases from 1.86 emu/cm^3 to 7.52 emu/cm^3 . However, coercivity value decreases from 202 Oe to 121 Oe by addition of Sm into

BLFO. At 5 K, the remanent magnetization increases from 2.46 emu/cm^3 to 2.6 emu/cm^3 with the addition of La into BFO. However, by Sm doping into BLFO, it increases from 2.6 emu/cm^3 to 12.9 emu/cm^3 , which is about 5 times than that of BLFO. Furthermore, the value of coercivity has been found to decrease from 523 Oe to 497 Oe with increase in Sm content from $y = 0$ to $y = 0.1$ as shown in Table 3. The improvement in magnetic parameters with Sm doping in BLFO leads to their potential use in applications associated with alternating fields.

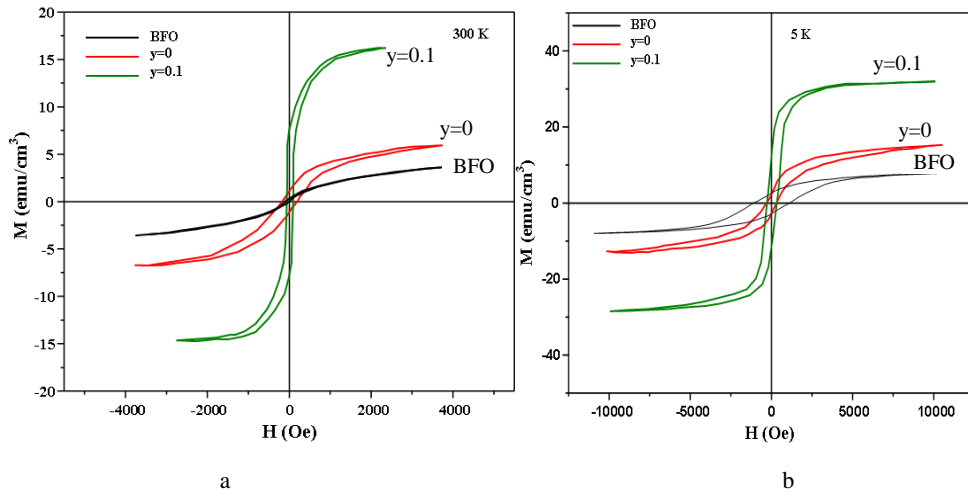


Fig. 6. M - H characteristics for BiFeO_3 and $\text{Bi}_{0.9-y}\text{Sm}_y\text{La}_{0.1}\text{FeO}_3$ thin films with $y = 0$ and $y = 0.1$ at different temperatures of (a) 300K and (b) 5K.

Table 3. Calculated M_S , M_R and H_C of BiFeO_3 and $\text{Bi}_{0.9-y}\text{Sm}_y\text{La}_{0.1}\text{FeO}_3$ thin films.

Sample	Temperature (K)	Saturation Magnetization (M_S) (emu/cm^3)	Remanent Magnetization (M_R) (emu/cm^3)	Coercivity (H_C) (Oe)
BiFeO_3	300	---	0.26	94
	5	7.5	2.46	920
$\text{Bi}_{0.9}\text{La}_{0.1}\text{FeO}_3$	300	6.8	1.86	202
	5	14.8	2.6	523
$\text{Bi}_{0.8}\text{Sm}_{0.1}\text{La}_{0.1}\text{FeO}_3$	300	17.5	7.52	121
	5	32.1	12.9	497

Fig. 7 shows the temperature variation of magnetization of BiFeO_3 and $\text{Bi}_{0.9-y}\text{Sm}_y\text{La}_{0.1}\text{FeO}_3$ thin films with $y = 0$ and $y = 0.1$ in the range 5K to 300K at an applied field (H) of 1000 Oe. We observe that La and Sm addition enhances the magnetism, but the enhancement is large in case of Sm doping in $\text{Bi}_{0.9}\text{La}_{0.1}\text{FeO}_3$. In these ZFC (zero field cooled) curves, a sharp cusp around 50K in case of $\text{Bi}_{0.9}\text{La}_{0.1}\text{FeO}_3$ has been observed which is similar to the blocking temperature T_B observed by M.K. Singh et

al [23]. This temperature is defined as a typical blocking process of an assembly of super-paramagnetic spins [24] and is qualitatively related to the presence of small particles, domains or domain walls in the system. However, the curve for $\text{Bi}_{0.8}\text{Sm}_{0.1}\text{La}_{0.1}\text{FeO}_3$ thin film shows no cusp, indicating an improved ferromagnetic behavior with large magnetization.

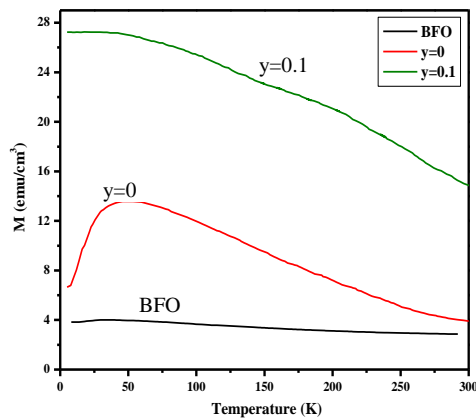


Fig. 7. *M-T characteristics for BiFeO₃ and Bi_{0.9-y}Sm_yLa_{0.1}FeO₃ thin films with $y = 0$ and $y = 0.1$ at applied field $H = 1000$ Oe.*

The enhancement of magnetic parameters with La and Sm addition is due to increased magnetoelectric coupling [25]. The antiferromagnetic ordering in the multiferroic BiFeO₃ is perpendicular to the ferroelectric polarization. The applied magnetic field causes the electric polarization in the sample due to magnetoelectric effect [26]. This ferroelectric polarization corresponds to a fictitious magnetic field along the direction of polarization; the sublattice spin will rotate symmetrically towards its direction under this effect. So the system takes on ferromagnetic ordering in the direction of ferroelectric ordering due to this magnetoelectric coupling. The ferroelectric polarization increases on La and Sm doping in BFO which enhances the magnetoelectric effect and hence the ferromagnetic ordering increases in BiFeO₃. Thus an increase in magnetism is achieved by La and Sm substitution due to increased magnetoelectric effect.

4. Conclusions

The BiFeO₃ and Bi_{0.9-y}Sm_yLa_{0.1}FeO₃ thin films with $y = 0, 0.02$ and 0.1 were grown on quartz substrate using pulsed laser deposition technique. XRD measurements shows the rhombohedral structure for the deposited films with highly oriented (110) diffraction peak. The La and Sm substitution at Bi site eliminated the small impurity phases of undoped BiFeO₃ and stabilized the crystal structure. Also, the Sm doping in BLFO leads to growth of low intensity (-220) and (010) peaks. The crystallite size of BLFO thin films calculated from XRD pattern was found to decrease with increase in Sm doping and is in agreement with AFM results. The study of optical properties revealed the decrease in refractive index with increase in Sm doping. The optical band gap was found to decrease from 2.66 eV to 2.54 eV with corresponding increase in Sm content from $y = 0$ to $y = 0.1$. Magnetic studies shows the ferromagnetism with Sm doping in BLFO with saturation magnetization 17.5 emu/cm³ and remanent magnetization 7.52 emu/cm³ in case of Bi_{0.9-y}Sm_yLa_{0.1}FeO₃ ($y = 0.1$) thin film at room temperature. However, antiferromagnetic behavior has

been found in case of BFO. The M-T curve shows a large enhancement in magnetism with Sm doping in BLFO thin films.

References

- [1] C. C. Lee, J. M. Wu, C. P. Hsiung, Appl. Phys. Lett. **90**, 182909 (2007).
- [2] Y. H. Lee, J. M. Wu, C. H. Lai, Appl. Phys. Lett. **88**, 042903 (2006).
- [3] F. Gao, C. Cai, Y. Wang, S. Dong, X. Qiu, G. Yuan, Z. Liu, J. Appl. Phys. **99**, 094105 (2006).
- [4] J. M. Moreau, C. Michel, R. Gerson, W. J. James, J. Phys. Chem. Solids **32**, 1315 (1971).
- [5] Y. H. Chu, L. W. Martin, M. B. Holcomb, R. Ramesh, Mater. Today **10**, 16 (2007).
- [6] V. R. Palkar, D. C. Kundaliya, S. K. Malik, S. Bhattacharaya, Phys. Rev. B **69**, 212102 (2004).
- [7] V. R. Palkar, D. C. Kundaliya, S. K. Malik, J. Appl. Phys. **93**, 4337 (2003).
- [8] S. T. Zhang, L. H. Pang, Y. Zhang, M. H. Lu, Y. F. Chen, J. Appl. Phys. **100**, 114108 (2006).
- [9] S. R. Das, P. Bhattacharya, R. N. Choudhary, J. Appl. Phys. **99**, 066107 (2006).
- [10] M. Mahesh, V. R. Palkar, Appl. Phys. Lett. **76**, 2764 (2000).
- [11] Y. Xu, M. Shen, Mater. Lett. **62**, 3600 (2008).
- [12] A. Z. Simoes, L. S. Cavalcante, C. S. Riccardi, J. A. Varela, E. Longo, Current Appl. Phys. **9**, 520 (2009).
- [13] A. Kaushal, D. Kaur, Solar Energy Mater. and Solar cells **93**, 193 (2009).
- [14] N. Kumar, A. Kaushal, C. Bhardwaj, D. Kaur, Optoelectron. Adv. Mater. - Rapid Commun. **4**, 1497 (2010).
- [15] V. R. Singh, A. Garg, D. C. Agrawal, Appl. Phys. Lett. **92**, 152905 (2008).
- [16] Z. Cheng, X. Wang, S. Dou, H. Kimura, K. Ozawa, Phys. Rev. B **77**, 092101 (2008).
- [17] B. D. Cullity, "Elements of X-Ray Diffraction", Addison-Wesley Publishing Co. Inc. (1982).
- [18] K. Singh, S. A. Acharya, S. S. Bhoga, Ionics **12**, 295 (2006).
- [19] R. Swanepoel, J. Phys. E: Sci. Instrum. **16**, 1214 (1983).
- [20] Z. S. El-Mandouh, M. S. Selim, Thin Solid Films **371**, 259 (2002).
- [21] S. Iakovlev, C. H. Solterbeck, M. Es-Souni, V. Zaporozhtchenko, Thin Solid Films **446**, 50 (2004).
- [22] J. Tauc, Amorphous and Liquid Semiconductor, Plenum Press, New York, p. 159 (1974).
- [23] M. K. Singh, W. Prellier, M. P. Singh, R. S. Katiyar, J. F. Scott, Phys. Rev. B **77**, 144403 (2008).
- [24] T. J. Park, G. C. Papaefthymiou, A. J. Viescas, A. R. Moodenbaugh, S. S. Wong, Nano Lett. **7**, 766 (2007).
- [25] N. Wang, J. Cheng, A. Pyatakov, A. K. Zvezdin, J. F. Li, L. E. Cross, D. Viehland, Phys. Rev. B **72**, 104434 (2005).
- [26] M. Fiebig, J. Phys. D: Appl. Phys. **38**, R123 (2005).

*Corresponding author: nearajbatra86@gmail.com